

Reconfigurable optomechanical circulator and directional amplifier

Zhen Shen, Yan-Lei Zhang, Yuan Chen, Fang-Wen Sun,^{*} Xu-Bo

Zou, Guang-Can Guo, Chang-Ling Zou,[†] and Chun-Hua Dong[‡]

*Key Laboratory of Quantum Information, Chinese Academy of Sciences,
University of Science and Technology of China, Hefei 230026, P. R. China. and
Synergetic Innovation Center of Quantum Information and Quantum Physics,
University of Science and Technology of China,
Hefei, Anhui 230026, P. R. China.*

Abstract

Non-reciprocal devices, which allow the non-reciprocal signal routing, serve as the fundamental elements in photonic and microwave circuits and are crucial in both classical and quantum information processing. The radiation-pressure-induced coupling between light and mechanical motion in traveling wave resonators has been exploited to break the Lorentz reciprocity, realizing non-reciprocal devices without magnetic materials. Here, we experimentally demonstrate a reconfigurable non-reciprocal device with alternative functions of either a circulator or a directional amplifier via the optomechanically induced coherent photon-phonon conversion or gain. The demonstrated device exhibits considerable flexibility and offers exciting opportunities for combining reconfigurability, non-reciprocity and active properties in single photonic structures, which can also be generalized to microwave as well as acoustic circuits.

^{*}Electronic address: fwsun@ustc.edu.cn

[†]Electronic address: clzou321@ustc.edu.cn

[‡]Electronic address: chunhua@ustc.edu.cn

The field of classical and quantum information processing with integrated photonics has achieved significant progresses during past decades, and most optical devices of the basic functionality have been realized [1]. Nonetheless, it is still a challenge to obtain devices with non-reciprocal or active gain properties. Especially the non-reciprocal devices, including the most common isolator and circulator, have attracted great efforts for both fundamental and practical considerations [2–7]. Although their bulky counterparts play a vital role in daily applications of optics, the requirement of strong external bias magnetic field and the magnetic field shields, and also the compatibility of lossy mageto-optics materials prevent the miniaturization [8].

Owing to the general principle of Lorentz reciprocity or time-reversal symmetry in optics, nonlinear optical effects are the remain option to come round the obstacle[9–11]. So far, the optical isolation based on spatiotemporal modulations and three-wave mixing effects have been developed [12–21], and the similar mechanism has been applied to superconducting microwave circuits [22–26]. Recently, the fiber-integrated optical circulator for single photon has also been realized, in which nonreciprocal behavior arises from the chiral interaction between the atom and the transversely confined light [27]. However, the optical circulator and the directional amplifier for large dynamic range of signal power is still inaccessible. Here, we demonstrate the first optomechanical circulator and directional amplifier in a two-tapered fiber coupled silica microresonator, which is used as an add-drop filter [28, 29]. Via a simple change in control field, this add-drop filter can be switched into circulator mode or directional amplifier mode. Our device has several advantages beyond its bulky counterparts, includes the reconfigurability, amplification, compactness.

The optomechanical circulator and directional amplifier feature the photonic structure as in Fig. 1A, where a silica microsphere resonator is evanescently coupled with two tapered microfibers (designated a and b) as signal input-output channels. For a passive configuration that without pump, it is a four-port add-drop filter device [28, 29], which can filter the signal from fiber a to b or vice versa via the passive cavity resonance. Because of the traveling wave nature, the microresonator supports pairs of degenerate clockwise (CW) and counter-clockwise (CCW) whispering-gallery modes, and the device transmission function is symmetric under the $1 \leftrightarrow 2$ and $4 \leftrightarrow 3$ commutation. The key to the reconfigurable

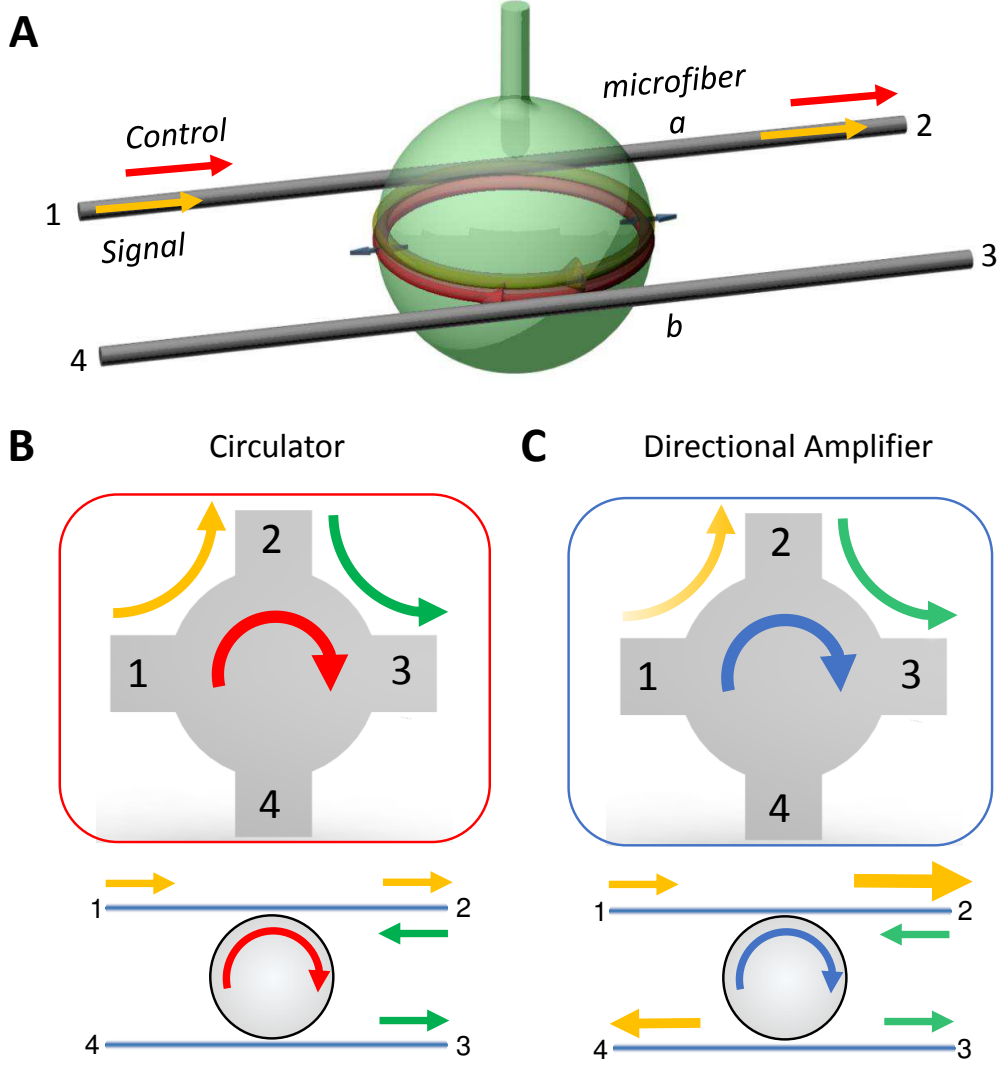


Figure 1: Schematic of the optomechanical circulator and directional amplifier. (A) The device consists of an optomechanical resonator and two coupled microfibers. A control field launched into port 1 excites the coupling between the mechanical motion and the clockwise optical field. (B and C) The routing direction of the signal light coincides with the control field (i.e., clockwise direction). The port number follows that of microfibers in (A). For the directional amplifier, the arrow color getting deeper (or size becoming larger) indicates gain in the corresponding direction, while the arrows remaining unchanged represent no gain.

non-reciprocity is the nonlinear optomechanical coupling, represented by the Hamiltonian

$$H_{int} = g_0(c_{cw}^\dagger c_{cw} + c_{ccw}^\dagger c_{ccw})(m + m^\dagger), \quad (1)$$

where $c_{cw(ccw)}$ and m denote the bosonic operators of the CW(CCW) optical cavity mode and

mechanical mode, respectively. The radial breathing mode that changes the circumference of the microsphere could modulate the cavity resonances, with the g_0 is the single-photon optomechanical coupling rate.

Biased by a control cavity field that detuned from the resonance, either the coherent conversion or the parametric coupling between the signal photon and phonon could be enhanced [30]. However, the bias control field can only stimulate the interaction between phonon and signal photon that propagating along the same direction as the bias. As a result of a directional control field, which is chosen as CW mode in our experiment, the time-reversal symmetry is broken and effective non-reciprocity is produced for the signal light. In particular, the device performs the function of either a circulator or a directional amplifier, which is determined by the frequency detuning of the control light with respect to the cavity resonance.

When the CW optical mode is excited via a red-detuned control field, i.e., $\omega_c - \omega_o \approx -\omega_m$, where ω_c , ω_o , ω_m are the respective frequencies of the control field, optical and mechanical modes, it gives rise to the well-known photon-phonon coherent conversion as a beam-splitter-like interaction ($c_{cw}^\dagger m + c_{cw} m^\dagger$) [31, 32]. For the CW signal photons sent to the cavity through the fiber port 1(3) in Fig. 1A, a transparent window appears in the transmittance from port 1(3) to port 4(2) when the signal is near resonance with the optical cavity mode. The signal is routed by the control field due to a destructive interference between the signal light and mechanically up-converted photons from the control field [31–33]. In contrast, for the two other input ports 2 and 4, the signal light couples to the CCW optical mode and drops to ports 3 and 1, respectively. Thus the add-drop functionality is remained for these two ports since the absence of optomechanical interaction. In general, the device functions as a four-port circulator, in which the signal entering any port is transmitted to the adjacent port in rotation, as shown in Fig. 1B.

For a control field that is blue-detuning from the CW mode ($\omega_c - \omega_o \approx \omega_m$), an effective photon-phonon pair generation process ($c_{cw}^\dagger m^\dagger + c_{cw} m$) leads to signal amplification. Similar to the case of circulator, only the signal that is launched into certain direction can couple with mechanical mode and be amplified, as shown in Figs. 1C. For example, signal input at port 1 leads to amplified signal output at both port 2 and 4. In reverse, signal input at port 2 will only drop to port 3 without amplification. Therefore, such a device can operate as an usual add-drop filter, circulator, or directional amplifier by programming the control field.

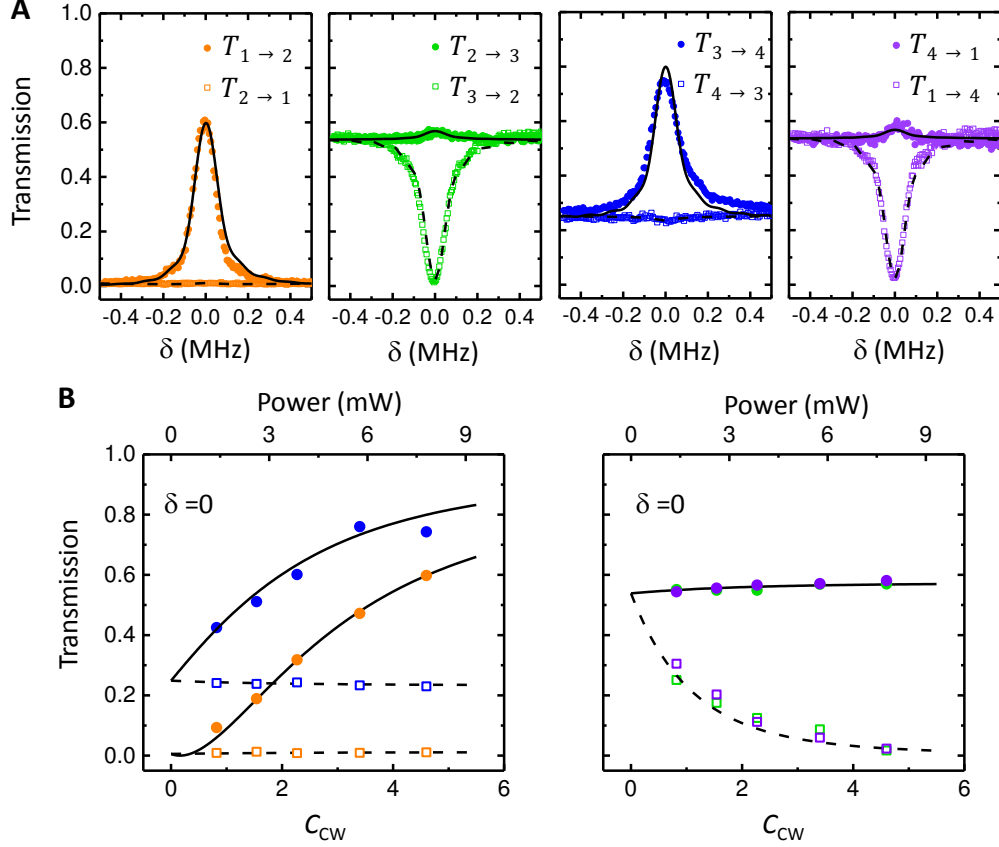


Figure 2: The demonstration of circulator function with red-detuned control field. (A) The measured port-to-port transmission spectra of signal around the cavity resonance, the solid circles for $T_{i \rightarrow i+1}$ and the open squares for $T_{i+1 \rightarrow i}$. The incident control power is 7.8 mW, corresponding to $C_{cw} = 4.6$. (B) The transmittance obtained at $\delta = 0$ versus C_{cw} . The lines in (A) and (B) are the theoretically expected values using the parameters $\kappa/2\pi = 16.2$ MHz, $\omega_m/2\pi = 90.47$ MHz, $\gamma/2\pi = 22$ kHz.

The optomechanical resonator used in this study is a silica microsphere with a diameter of around $35 \mu\text{m}$, where we choose a high-Q-factor whispering-galley mode with intrinsic damping rate $\kappa_0/2\pi = 3$ MHz near 780 nm. The radial breathing mechanical mode has a frequency of $\omega_m/2\pi = 90.47$ MHz and a dissipation rate of $\gamma/2\pi = 22$ kHz. The two microfibers are mounted in two 3D stages and the distance between the resonator and microfibers is fixed throughout the experiment, and the external coupling rates of the two channels are $\kappa_a/2\pi = 9$ MHz and $\kappa_b/2\pi = 4.2$ MHz, respectively (see [34] for more details about the setup).

For the experimental demonstration of optomechanical circulator, we first measure the

signal transmission spectra $T_{i \rightarrow i+1}$ from i -th to $(i+1)$ -th port and the reversal $T_{i+1 \rightarrow i}$ with $i \in \{1, 2, 3, 4\}$ (as shown in Fig. 2A) when the CW optical mode is excited by a red-detuned control laser. Here, the control laser and signal light are pulsed (pulse width $\tau = 10 \mu\text{s}$) to avoid the thermal instability of the microsphere [19, 33]. With the detuning δ between the signal and cavity field (see [34] for more spectra), the spectra unambiguously present asymmetric transmittance in the forward ($i \rightarrow i+1$) and backward ($i+1 \rightarrow i$) directions around $\delta \approx 0$: relatively high forward transmittance (60% \sim 80%) while near-zero backward transmittance. Such performance indicates an optical circulator (Fig. 1B) with insertion loss of around 1 \sim 2 dB. The isolation for the backward $T_{4 \rightarrow 3}$ is slightly higher, because of the imperfection imposed by the unbalanced external coupling rates of two channels. To achieve a better understanding of the role of the optomechanical interactions, we measure the transmission spectra under different intensities of the control field. The transmissions at $\delta = 0$ are summarized and plotted in Fig. 2B as a function of the cooperativity $C_{\text{cw}} \equiv 4g_0^2 N_d / \kappa \gamma$, where N_d is the CW intracavity control photon number, and $\kappa = \kappa_0 + \kappa_a + \kappa_b$ is the total cavity damping rate. By increasing C_{cw} , we observe the non-reciprocal transmittance contrast between forward and backward directions ($T_{i \rightarrow i+1} - T_{i+1 \rightarrow i}$) increases from 0 to around 60.

By tuning the frequency of control field to the upper motional sideband of the optical mode ($\omega_c - \omega_0 = \omega_m$) and keeping other conditions the same as before, the same device is reconfigured to be a directional amplifier. As shown in Fig. 3A, only the signal light launched into port 1 and port 3 (i.e., coupled to CW mode) will be simultaneously transferred to port 2 and port 4 with considerable gain, but not vice versa (see [34] for more spectra). For the channel from port 2 to port 1, the lower transmittance predicted by theory at $\delta = 0$ is not measured due to the noise. Here, the experimental results are fitted to the transient transmission spectra, the sinc-function-like oscillations around the central peak are observed due to the impulse response of the device for a 10 μs rectangular control pulse. For the transmittance at $\delta = 0$ and $C_{\text{cw}} = -4.0$, where the negative sign of cooperativity represents the blue-detuned drive [19], the signal field from port 1 to port 2 is amplified by 15.2 dB but in the reversed direction it suffers 19.1 dB loss as shown in Fig. 3B. Hence, the maximum contrast ratio between forward and backward probe transmission is approximately 34.3 dB when $C_{\text{cw}} = -4.0$.

To fully characterize the performance of our reconfigurable non-reciprocal devices, we

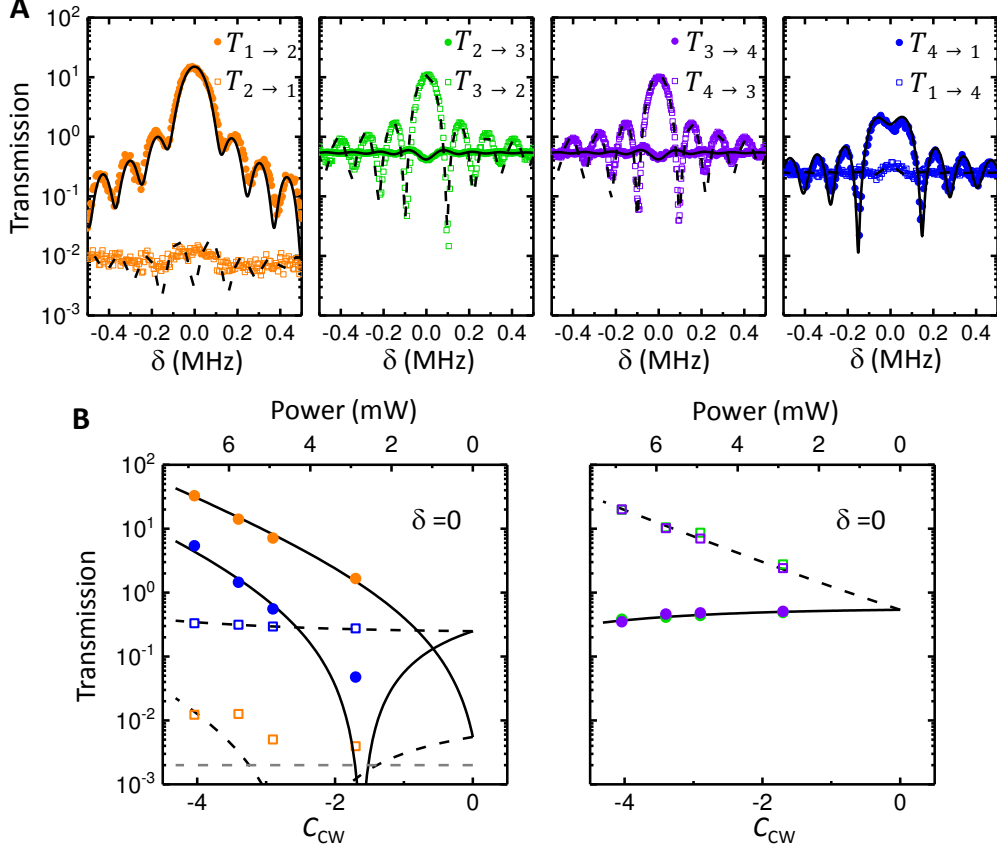


Figure 3: The demonstration of directional amplifier with blue-detuned control field. (A) The typical measured transmission spectra for the function of directional amplifier. The solid circles represent $T_{i \rightarrow i+1}$ and the open squares represent $T_{i+1 \rightarrow i}$. The incident control power is 5.8 mW, corresponding to $C_{cw} = -3.4$. (B) The transmittance obtained at $\delta = 0$ versus C_{cw} . The lines in (A) and (B) are the theoretically expected values using the parameters $\kappa/2\pi = 16.2$ MHz, $\omega_m/2\pi = 90.47$ MHz, $\gamma/2\pi = 22$ kHz.

measure the complete transmission spectra $T_{i \rightarrow j}$ between all ports (i.e., $i, j \in \{1, 2, 3, 4\}$), with $C_{cw} = 0$ for add-drop filter, $C_{cw} > 0$ for circulator and $C_{cw} < 0$ for directional amplifier, respectively. Figure 4 shows the experimental results of the transmittance matrix for $C_{cw} = 0, 4.6, -4.0$ at $\delta = 0$, and also the matrix for ideal circulator as a comparison. To quantify the device performance, we introduce the ideality metric $I = 1 - \frac{1}{8} \sum_{i,j} |T_{i \rightarrow j}^N - T_{i \rightarrow j}^I|$, with $T_{i \rightarrow j}^N = T_{i \rightarrow j}/\eta_i$ is the normalized experimental transmittance at $\delta = 0$ for subtracting the influence of the insertion loss (see [34] for more details), $T_{i \rightarrow j}^I$ for ideal performance and $\eta_i = \sum_j T_{i \rightarrow j}$ is total output for the signal field entering port i . As shown in Fig. 4E, the ideality of circulator and amplifier approaches unity with increasing $|C_{cw}|$, which agrees well

with theoretical fittings [34]. The best idealities of all three functions of the device exceed 75.

The demonstrated non-reciprocal circulator and amplifier based on the optomechanical interaction in traveling-wave resonator enables versatile photonic elements, and offers the unique advantages of all-optical switching, non-reciprocal routing and amplification. Other promising applications along this direction including the non-reciprocal frequency conversion, narrowband reflector, as well as synthetic magnetic field for light by exploiting multiple optical modes in single cavity [19, 21, 35]. With the advances of material and nanofabrication, these devices will be implemented in photonic integrated circuits [36], which allows stronger optomechanical interaction and smaller device footprint. Then, the missing block of non-reciprocity could then be tailored and implemented to meet specific experimental demands. The principle demonstrated here can also be incorporated into microwave superconducting devices as well as the acoustic devices in the emerging research field of quantum phononics [37].

Note added: During the preparation of this manuscript, a similar work by F. Ruesink et al. has been reported on the arXiv [38], where an optical circulator based on microtoroid resonator was demonstrated.

Acknowledgments

The work was supported by the National Key R&D Program of China (Grant No.2016YFA0301303, 2016YFA0301700), the Strategic Priority Research Program (B) of the Chinese Academy of Sciences (Grant No. XDB01030200), the National Natural Science Foundation of China (Grant No.61575184, and No. 11722436), the Fundamental Research Funds for the Central Universities. This work was partially carried out at the USTC Center for Micro and Nanoscale Research and Fabrication.

Author contributions

Z.S., Y.-L.Z. and Y.C. contribute equally to this work. Z.S., C.-H.D. and C.-L.Z conceived the experiments, Z.S., Y.C. and C.-H.D. prepared microsphere, built the experimental setup and carried out measurements. Y.-L.Z., Z.S. and Y.C. performed the numerical simulation and analyzed the data, X.-B.Z. and F.W.S. provided theoretical support. Z.S., C.-H.D. and C.-L.Z. wrote the manuscript with input from all co-authors. C.-H.D., F.-W.S. and

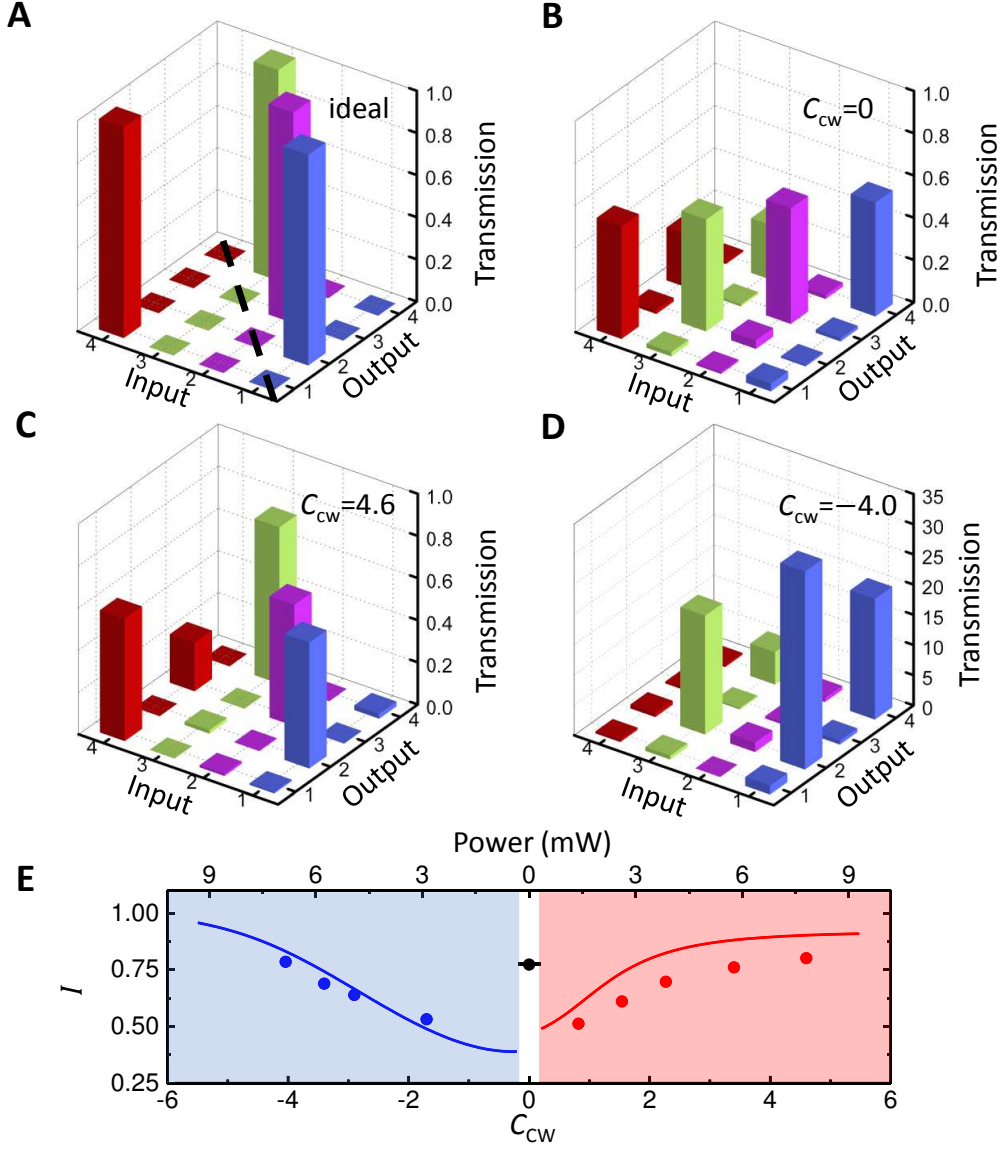


Figure 4: Transmission matrices. (A) The transmission matrix of an ideal circulator: only $T_{1 \rightarrow 2} = T_{2 \rightarrow 3} = T_{3 \rightarrow 4} = T_{4 \rightarrow 1} = 1$ and all remaining matrix elements are 0. An circulator requires an asymmetric transmission matrix with regard to the dashed line, which breaks the reciprocity. Conversely, (B) shows a symmetric transmission matrix measured without control field, representing a reciprocal device. (C and D) The transmission matrix for the demonstrated circulator and directional amplifier, respectively. The control power is 7.8 mW for circulator and 6.9 mW for directional amplifier, corresponding to $C_{cw} = 4.6$ and -4.0 . The values of all transmission matrix are provided in Supplementary Information. (E) Identical I of circulator, directional amplifier and add-drop filter as a function of C_{cw} . The lines are the results of theoretical calculations.

G.-C.G. supervised the project. All authors contributed extensively to the work presented in this paper.

Additional information

Supplementary information is available in the online version of the paper. Reprints and permissions information is available online at. Correspondence and requests for materials should be addressed to F.-W. S., C.-L. Z or C.-H. D.

Competing financial interests

The authors declare no competing financial interests.

-
- [1] B. E. A. Saleh and M. C. Teich, “Fundamentals of Photonics, 2nd Edition,” ISBN: 978-0-471-35832-9, (2007).
 - [2] Y. Shoji and T. Mizumoto, “Magneto-optical nonreciprocal devices in silicon photonics,” *Sci. Technol. Adv. Mater.* **15**, 014602 (2014).
 - [3] A. Metelmann and A. A. Clerk, “Nonreciprocal photon transmission and amplification via reservoir engineering,” *Phys. Rev. X* **5**, 021025 (2015).
 - [4] P. Lodahl, S. Mahmoodian, S. Stobbe, P. Schneeweiss, J. Volz, A. Rauschenbeutel, H. Pichler, and P. Zoller, “Chiral quantum optics,” *Nature* **541**, 473-480 (2017).
 - [5] A. Kamal and A. Metelmann, “Minimal models for nonreciprocal amplification using biharmonic drives,” *Phys. Rev. Appl.* **7**, 034031 (2017).
 - [6] Y. Li, Y. Y. Huang, X. Z. Zhang, and L. Tian, “Optical directional amplification in a three-mode optomechanical system,” *Opt. Express* **25**, 18907-18916 (2017).
 - [7] D. Malz, L. D. Tóth, N. R. Bernier, A. K. Feofanov, T. J. Kippenberg, and A. Nunnenkamp, “Quantum-limited directional amplifiers with optomechanics,” arXiv:1705.00436, 2017.
 - [8] L. Bi, J. Hu, P. Jiang, D. H. Kim, G. F. Dionne, L. C. Kimerling, and C. A. Ross, “On-chip optical isolation in monolithically integrated non-reciprocal optical resonators,” *Nat. Photon.* **5**, 758–762 (2011).
 - [9] Z. Yu and S. Fan, “Complete optical isolation created by indirect interband photonic transitions,” *Nat. Photon.* **3**, 91–94 (2009).

- [10] Y. Shi, Z. Yu, and S. Fan, “Limitations of nonlinear optical isolators due to dynamic reciprocity,” *Nat. Photon.* **9**, 388-392 (2015).
- [11] L. D. Tzuang, K. Fang, P. Nussenzevige, S. Fan, and M. Lipson, “Non-reciprocal phase shift induced by an effective magnetic flux for light,” *Nat. Photon.* **8**, 701–705 (2014).
- [12] M. S. Kang, A. Butsch, and P. S. J. Russell, “Reconfigurable light-driven opto-acoustic isolators in photonic crystal fibre,” *Nat. Photon.* **5**, 549–553 (2011).
- [13] C.-H. Dong, Z. Shen, C.-L. Zou, Y.-L. Zhang, W. Fu, and G.-C. Guo, “Brillouin-scattering-induced transparency and non-reciprocal light storage,” *Nat. Commun.* **6**, 6193 (2015).
- [14] J. Kim, M. C. Kuzyk, K. Han, H. Wang, and G. Bahl, “Non-reciprocal Brillouin scattering induced transparency,” *Nat. Phys.* **11**, 275–280 (2015).
- [15] X. Guo, C.-L. Zou, H. Jung, and H. X. Tang, “On-chip strong coupling and efficient frequency conversion between telecom and visible optical modes,” *Phys. Rev. Lett.* **117**, 123902 (2016).
- [16] Y. Zheng, J. Yang, Z. Shen, J. Cao, X. Chen, X. Liang, and W. Wan, “Optically Induced Transparency in a micro-cavity,” *Light: Sci. & App.* **5**, e16072 (2016).
- [17] S. Hua, J. Wen, X. Jiang, Q. Hua, L. Jiang, and M. Xiao, “Demonstration of a chip-based optical isolator with parametric amplification,” *Nat. Commun.* **7**, 13657 (2016).
- [18] M. Hafezi and P. Rabl, “Optomechanically induced nonreciprocity in microring resonators,” *Optics Express* **20**, 7672 (2012).
- [19] Z. Shen, Y.-L. Zhang, Y. Chen, C.-L. Zou, Y.-F. Xiao, X.-B. Zou, F.-W. Sun, G.-C. Guo, and C.-H. Dong, “Experimental realization of optomechanically induced non-reciprocity,” *Nat. Photon.* **10**, 657–661 (2016).
- [20] F. Ruesink, M.-A. Miri, A. Alù, and E. Verhagen, “Nonreciprocity and magnetic-free isolation based on optomechanical interactions,” *Nat. Commun.* **7**, 13662 (2016).
- [21] K. Fang, J. Luo, A. Metelmann, M. H. Matheny, F. Marquardt, A. A. Clerk, and O. Painter, “Generalized nonreciprocity in an optomechanical circuit via synthetic magnetism and reservoir engineering,” *Nat. Phys.* **13**, 465–471 (2017).
- [22] D. M. Pozar, “*Microwave Engineering*,” 3rd ed. (John Wiley and Sons, Inc., Hoboken, NJ, 2005).
- [23] K. M. Sliwa, M. Hatridge, A. Narla, S. Shankar, L. Frunzio, R. J. Schoelkopf, and M. H. Devoret, “Reconfigurable Josephson circulator/directional amplifier,” *Phys. Rev. X* **5**, 041020 (2015).

- [24] G. A. Peterson, F. Lecocq, K. Cicak, R. W. Simmonds, J. Aumentado, and J. D. Teufel, “Demonstration of efficient nonreciprocity in a microwave optomechanical circuit,” *Phys. Rev. X* **7**, 031001 (2017).
- [25] S. Barzanjeh, M. Wulf, M. Peruzzo, M. Kalaei, P. B. Dieterle, O. Painter, and J. M. Fink, “Mechanical On-Chip Microwave Circulator,” arXiv:1706.00376, 2017.
- [26] N. R. Bernier, L. D. Tóth, A. Koottandavida, M. Ioannou, D. Malz, A. Nunnenkamp, A. K. Feofanov, and T. J. Kippenberg, “Nonreciprocal reconfigurable microwave optomechanical circuit,” arXiv:1612.08223, 2017.
- [27] M. Scheucher, A. Hilico, E. Will, J. Volz, and A. Rauschenbeutel, “Quantum optical circulator controlled by a single chirally coupled atom,” *Science* **354**, 1577-1580 (2016).
- [28] M. Cai, G. Hunziker, and K. J. Vahala, “Fiber-optic add-drop device based on a silica microsphere-whispering gallery mode system,” *IEEE Photon. Technol. Lett.* **11**, 686-687 (1999).
- [29] F. Monifi, J. Friedlein, Ş. K. Özdemir, and L. Yang, “A robust and tunable add-drop filter using whispering gallery mode microtoroid resonator,” *J. Lightwave Technol.* **30**, 3306-3315 (2012).
- [30] M. Aspelmeyer, T. J. Kippenberg, and F. Marquardt, “Cavity optomechanics,” *Rev. Mod. Phys.* **86**, 1391 (2014).
- [31] S. Weis, R. Rivière, S. Deléglise, E. Gavartin, O. Arcizet, A. Schliesser, and T. J. Kippenberg, “Optomechanically induced transparency,” *Science* **330**, 1520 (2010).
- [32] A. H. Safavi-Naeini, T. P. M. Alegre, J. Chan, M. Eichenfield, M. Winger, Q. Lin, J. T. Hill, D. E. Chang, and O. Painter, “Electromagnetically induced transparency and slow light with optomechanics,” *Nature* **472**, 69–73 (2011).
- [33] C. Dong, V. Fiore, M. C. Kuzyk, and H. Wang, “Optomechanical dark mode,” *Science* **338**, 1609–1613 (2012).
- [34] Materials and methods are available online as supplementary materials.
- [35] Y.-L. Zhang, C.-H. Dong, C.-L. Zou, X.-B. Zou, Y.-D. Wang, and G.-C. Guo, “Optomechanical devices based on traveling-wave microresonators,” *Phys. Rev. A* **95**, 043815 (2017).
- [36] J. D. Cohen, S. M. Meenehan, G. S. MacCabe, S. Gröblacher, A. H. Safavi-Naeini, F. Marsili, M. D. Shaw, and Oskar Painter, “Phonon counting and intensity interferometry of a nanomechanical resonator,” *Nature* **520**, 522–525 (2015).
- [37] M. V. Gustafsson, T. Aref, A. F. Kockum, M. K. Ekstrom, G. Johansson, and P. Delsing,

“Propagating phonons coupled to an artificial atom,” *Science* **346**, 207–211 (2014).

- [38] F. Ruesink, J. P. Mathew, M.-A. Miri, A. Alù, and E. Verhagen, “Optical circulation in a multimode optomechanical resonator,” arXiv:1708.07792, 2017.